PAPER

Unveiling of Terahertz Emission from Ultrafast Demagnetization and the Anomalous Hall Effect in a Single Ferromagnetic Film

Unveiling of Terahertz Emission from Ultrafast Demagnetization and the Anomalous Hall Effect in a Single Ferromagnetic Film

Zhiqiang Lan(蓝志强), Zhangshun Li(李章顺), Haoran Xu(徐浩然), Fan Liu(刘凡), Zuanming Jin(金钻明)*, Yan Peng(彭滟), and Yiming Zhu(朱亦鸣)

Terahertz Technology Innovation Research Institute, Terahertz Spectrum and Imaging Technology Cooperative Innovation Center, Shanghai Key Lab of Modern Optical System, University of Shanghai for Science and Technology, Shanghai 200093, China

(Received 29 January 2024; accepted manuscript online 12 March 2024)

Using THz emission spectroscopy, we investigate the elementary spin dynamics in ferromagnetic single-layer Fe on a sub-picosecond timescale. We demonstrate that THz radiation changes its polarity with reversal of the magnetization applied by the external magnetic field. In addition, it is found that the sign of THz polarity excited from different sides is defined by the thickness of the Fe layer and Fe/dielectric interface. Based on the thickness and symmetry dependences of THz emission, we experimentally distinguish between the two major contributions: ultrafast demagnetization and the anomalous Hall effect. Our experimental results not only enrich understanding of THz electromagnetic generation induced by femtosecond laser pulses but also provide a practical way to access laser-induced ultrafast spin dynamics in magnetic structures.

DOI: 10.1088/0256-307X/41/4/044203

In recent years, laser-induced ultrafast magnetization dynamics in matter has attracted strong basic theoretical and technological interest.[1–7] Indeed, the ability to efficiently modify the magnetization of ferromagnetic (FM) metals on a femtosecond timescale paves the way to practical applications for ultrafast optical writing of magnetic memories and magnetic data storage and manipulation.[8,9] Although many interesting theories and experimental explanations have been presented, a clear physical picture of the processes occurring during the interaction of ultrashort laser pulses with spin order remains unclear.[10–14]

THz radiation is the part of electromagnetic spectrum that lies between microwave and far-infrared radiation.[15–18] In general, the THz frequency range spans from 0.1 to 10 THz. THz radiation has become an increasingly important area of research owing to its potential applications in various fields such as biomedicine, security, and metamaterial sensors.[19–24] Recently, several experiments have shown that THz emission spectroscopy provides the opportunity for investigating the spin dynamics in antiferromagnetic[25–27] and FM heterostructures.[28–31] THz emission spectroscopy is based on the following principle: an ultrashort laser pulse excites a transient spin current and/or magnetic dipole in the sample, which in turn acts as a source of electromagnetic radiation emitted from the sample into free space. In the case of sub-picosecond dynamics of the laser-induced electronic and/or magnetic dipole, the frequency of emitted electromagnetic radiation falls into the THz range.[32,33]

In 2004, Beaurepaire *et al.* first discovered that ultrafast demagnetization (UDM) of Ni can generate THz radiation, and it is proportional to the second time derivative of the magnetization and is described by the three-temperature model.[1,2] In 2020, Zhang *et al.* demonstrated a method for ultrafast THz magnetometry which directly accessed the ultrafast magnetization dynamics in a single-layer Fe film.[34] Kampfrath *et al.* discovered the spin-to-charge conversion mechanisms in FM and nonmagnetic heterostructures for THz emission,[35] including the inverse spin Hall effect (ISHE)[36] and inverse Rashba–Edelstein effect.[37,38] In contrast to the mentioned mechanisms, the anomalous Hall effect (AHE) was also demonstrated to generate THz radiation in a single FM layer without a nonmagnetic layer or Rashba interface.[39–41] The AHE mechanism involves the generation of backflow charge current from the FM layer/dielectric interface and subsequent conversion to a transverse transient charge current.[42,43] Recently, Liu *et al.* analyzed the difference between the THz emission from the capping and substrate sides of CoFeB films and demonstrated that the contributions of AHE and UDM are $\sim$93% and $\sim$7% compared to the THz emission, respectively.[40] However, for a thicker FM film, THz emission was found to be dominant due to the photo-induced UDM.[44] Note that for various samples with different thicknesses the ratio of UDM and AHE mechanisms should be different, but a systematic study demonstrating the relationship between UDM and AHE is still missing.

In this Letter, we employ a method of THz emission spectroscopy to investigate the spin dynamics in laser-excited FM Fe nanometer films. We investigate the ef-

*Corresponding author. Email: physics_jzm@usst.edu.cn

fect of magnetic field, photo-excitation symmetry, and Fe thickness dependence on the THz emission. We distinguish the different contributions to the THz radiation from the UDM and AHE mechanisms. The THz amplitude with the UDM mechanism (magnetic dipole) is linearly dependent on the thickness of the Fe layer. The emitted THz amplitude with the AHE mechanism (electric dipole) increases with increase in Fe layer thickness up to about 5 nm. When the thickness is greater than 5 nm, the THz emission decreases with increasing thickness. In the present case, the anomalous Nernst effect (ANE) cannot be directly observed when the sample is pumped by a Ti:sapphire regenerative amplifier.

Preparation of Samples. Thin films of Fe with different thicknesses were deposited on MgO (001) substrates at room temperature using DC magnetron sputtering. All the Fe films were covered by a 5-nm-thick SiO_2 capping layer grown by radio-frequency magnetron sputtering. The base pressure of the sputter chamber was 5×10^{-5} Pa.

Experimental Setup. To capture the features of the emitted THz radiation from single-layer Fe we performed the THz emission experiment shown in Fig. 1(a). The Fe layer samples were photo-excited and the THz pulses were emitted through the sample on a MgO substrate. A Ti:sapphire laser delivered pulses of 120 fs duration with a central wavelength of 800 nm and repetition rate of 1 kHz. A 1-mm-thick ⟨110⟩ ZnTe crystal acted as a detector for the THz pulses using electro-optic sampling (EOS). A static in-plane magnetic field of $H = 200$ mT (along the x-axis) was used to saturate the magnetization of all Fe films. All measurements were purged with dry air to avoid absorption of water vapor at room temperature. The normal-incidence excitation configuration excludes the contribution of magnetically enhanced surface nonlinearity to the observed THz emission.[45] Details of the THz emission spectroscopy are described elsewhere.[46]

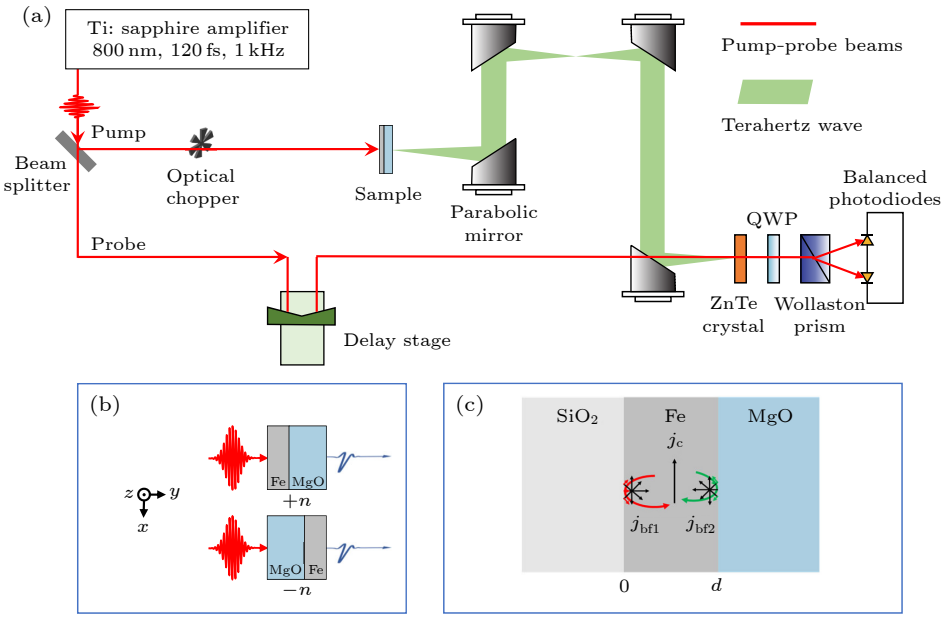

Fig. 1. (a) Schematic of THz emission spectroscopy. (b) THz emission with excitations from the FM side ($+n$) and MgO side ($-n$), respectively. The SiO_2 capping layer is omitted for simplicity. (c) Schematic of the AHE-based THz emission mechanism of single-layer Fe.

Experimental Data Analysis. Figure 2 plots the generated THz pulses from a MgO/Fe sample with opposite magnetization directions ($\pm H$) and photo-exciting sides ($\pm n$) when the single-layer Fe is irradiated by the amplifier laser pulse normally. Figure 2(a) shows the typical time-domain THz emission signals, $\boldsymbol{E}_{\rm EOS}(t)$, generated from MgO/Fe (30 nm). Both $\boldsymbol{E}_{\rm EOS}(t)$ are inverted symmetrically as the direction of sample magnetization $\boldsymbol{M}$ is reversed with an external magnetic field of $\pm H = \pm 200$ mT (sufficient to saturate the Fe film). It is important to note that the polarization of the emitted THz pulses is along the z-axis and the component along the x-axis is negligible. The polarization of THz generation follows the direction perpendicular to $\boldsymbol{M}$. It can be seen that the polarity of the THz waveform is the same when the sample is flipped from $+n$ to $-n$. The THz waveform is delayed when the sample is pumped from the Fe side ($+n$) due to the increase in the optical path by the 0.5 mm thick MgO substrate for THz pulse propagation. Thus, the THz emission from a 30-nm-thick Fe film is mainly attributed to UDM, described as time-resolved magnetic dipole radiation. The polarity of THz waveforms is expected to be the same, because the dynamics of UDM does not change for both MgO substrate and Fe film side pumping when the external magnetic field is fixed.

It should be noted that the experimental result is dif-

ferent for the THz emission from 3-nm-thick Fe film, as shown in Fig. 2(b). The polarity of the THz emission is reversed when the magnetization direction is reversed, while the polarity of the THz waveform is reversed when the sample is flipped, indicating a feature of in-plane charge currents resulting from the spin-to-charge conversion.[46] It can also be found that the polarities of THz emission in the 30 nm and 3 nm samples are opposite when pumped from the FM side while keeping the magnetization direction the same. The THz emission result depends sensitively on both the pumping configuration and the thickness of the sample. Note that the THz emission due to the ISHE mechanism is expected to be neglected since there is no heavy metal with high spin-to-charge conversion efficiency in our samples. Figure 2(c) shows the results for the THz waveforms of the 3-nm-thick sample with laser excitation varied from 0.2 mJ·cm^{-2} to 4.1 mJ·cm^{-2}. Figure 2(d) shows the linear dependence of the peak amplitude of THz emission on the pump fluence for different Fe single layer thicknesses (3 nm, 4 nm, 5 nm, 7 nm, 10 nm, and 12 nm). It should also be noted that the THz peak amplitude variation with respect to the pump fluences for samples with different thickness shows different proportional trends, which suggests that the measured THz emission originates from a combination of UDM and the AHE, as explained later.

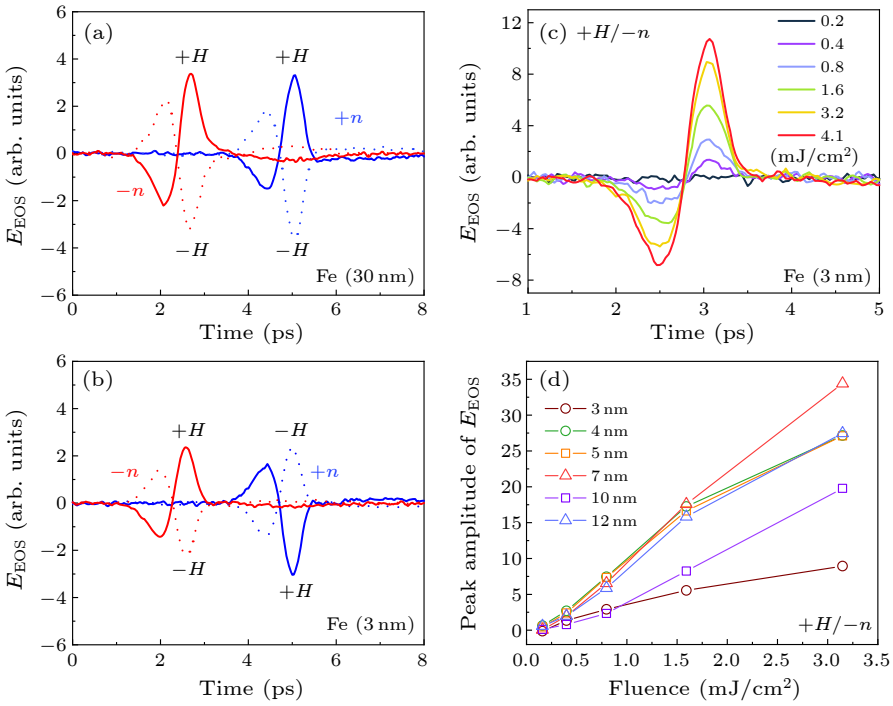

Fig. 2. (a) THz emission waveforms from 30-nm-thick Fe film. (b) THz emission waveforms from 3-nm-thick Fe film. The blue waveforms are for FM side pumping ($+n$); the red waveforms are for MgO side pumping ($-n$); solid lines are for a positive magnetic field ($+H$); dashed lines are for negative magnetic field ($-H$). (c) Measured THz waveforms as a function of pump fluence. (d) THz peak amplitude for Fe films as functions of pump fluence.

Let us discuss the distinctive features of THz generation from UDM and the AHE. Upon excitation by 800 nm pump light, the laser-excited hot electrons in Fe excite nonequilibrium magnons and generate a transient spin voltage $\dot{M} \propto j_s \propto \mu^{\uparrow} - \mu^{\downarrow}$, where $\mu^{\uparrow}$ and $\mu^{\downarrow}$ are the chemical potentials of majority- and minority-spin electrons in the FM layer, respectively.[47,48] These processes in turn drive ultrafast demagnetization, which induces THz generation, $E_{\mathrm{THz}}^{\mathrm{UDM}}(t) \propto \frac{\partial^2 \boldsymbol{M}(t)}{\partial t^2}$. The polarity of $E_{\mathrm{THz}}^{\mathrm{UDM}}(t)$ is independent of the FM side and MgO side pumping. For AHE-induced THz emission it was attributed to the conversion of the laser-excited net backflow current (longitudinal) to a transient transverse current.[39] As shown in Fig. 1(c), due to the different interfaces, the backflow currents of $\boldsymbol{j}_{\mathrm{bf1}}$ and $\boldsymbol{j}_{\mathrm{bf2}}$ from the Fe/SiO_2 capping layer and MgO substrate/Fe interfaces, respectively, will not be canceled out. This leads to a net backflow longitudinal current $\boldsymbol{j}_{\mathrm{bf}} = \boldsymbol{j}_{\mathrm{bf1}} - \boldsymbol{j}_{\mathrm{bf2}}$ along the film thickness direction. According to the AHE, $\boldsymbol{j}_{\mathrm{bf}}(t)$ can be converted to a transient charge current $\boldsymbol{j}_{\mathrm{c}}(t) = \theta_{\mathrm{AHE}}(\boldsymbol{j}_{\mathrm{bf}}(t) \times \frac{\boldsymbol{M}}{|\boldsymbol{M}|})$, where θ_{AHE} and $\frac{\boldsymbol{M}}{|\boldsymbol{M}|}$ are the anomalous Hall angle and the magnetization direction of Fe films, respectively. Thereby, $\boldsymbol{j}_{\mathrm{c}}(t)$ emits a THz pulse, $E_{\mathrm{THz}}^{\mathrm{AHE}}(t) \propto \frac{\partial}{\partial t}[\boldsymbol{j}_{\mathrm{c}}(t)]$. The polarity of $E_{\mathrm{THz}}^{\mathrm{AHE}}(t)$ is reversed upon flipping the pumping side from the MgO side to the FM side. $\boldsymbol{j}_{\mathrm{bf}}(t)$ depends on the dielectric properties of the interfaces, such as roughness, crystal structure and interface intermixing.

To distinguish the contributions of UDM and the AHE to THz emission in single-layer Fe film, we performed thickness-dependent measurements under four different

configurations (i.e., $\pm n$ and $\pm H$) in Fig. 3. The pump fluence was fixed at 0.8 mJ·cm^{-2}. Figures 3(a) and 3(b) depict the THz waveforms from Fe films (thickness varying from 2 nm to 30 nm) with FM side pumping for $+H$ and $-H$, respectively. Figures 3(c) and 3(d) show the THz waveforms from Fe films with substrate side pumping for $+H$ and $-H$, respectively. Below a thickness of 3 nm, the laser-induced THz emission is barely noticeable. It is important to see that the amplitude and phase of the emitted THz waveforms are strongly dependent on the thickness of sample. The 5-nm-thick film has the maximum THz emission amplitude. The polarities of the THz waveforms in 5 nm and 30-nm-thick films are reversed for comparison, as shown in Figs. 3(a) and 3(b).

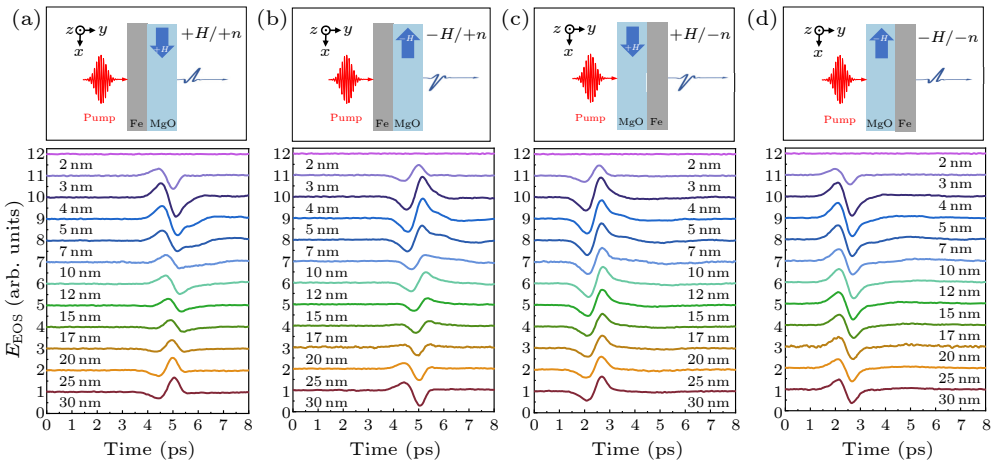

Fig. 3. Thickness dependence of THz waveforms from Fe single layers at (a) $+H/+n$, (b) $-H/+n$, (c) $+H/-n$, (d) $-H/-n$. The THz waveforms are shifted on the y-axis for clarity.

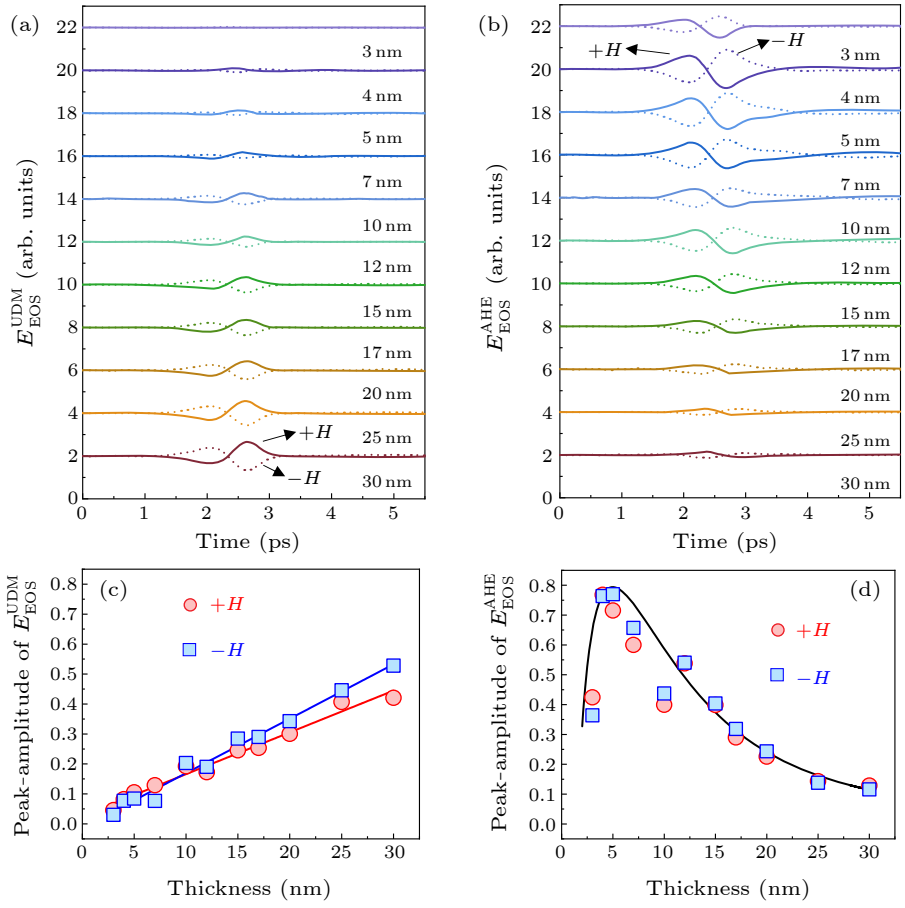

Fig. 4. Thickness dependences of THz contributions from (a) UDM and (b) AHE mechanisms in single-layer Fe. The THz waveforms are shifted on the y-axis for clarity (solid lines, $+H$; dashed lines, $-H$). The peak amplitudes of (c) $\boldsymbol{E}_{EOS}^{UDM}$ and (d) $\boldsymbol{E}_{EOS}^{AHE}$ as functions of Fe thickness with $\pm H$. The solid lines are guides to the eyes.

The THz waveforms from Fe thin films include contributions from both UDM and the AHE. As mentioned above, the polarity of the THz emission by the AHE is opposite for pumping from the substrate side and from the FM layer side, while the contribution from UDM does not change under the same magnetization. Thus, $\boldsymbol{E}^{+n}_{\rm EOS}(t) = \boldsymbol{E}^{\rm UDM}_{\rm EOS}(t) + \boldsymbol{E}^{\rm AHE}_{\rm EOS}(t)$ and $\boldsymbol{E}^{-n}_{\rm EOS}(t) = \boldsymbol{E}^{\rm UDM}_{\rm EOS}(t) - \boldsymbol{E}^{\rm AHE}_{\rm EOS}(t)$. Consequently, the distinct contributions of UDM- and AHE-based THz emission can be extracted by

$$\boldsymbol{E}^{\rm UDM}_{\rm EOS}(t) = \frac{1}{2}[\boldsymbol{E}^{+n}_{\rm EOS}(t) + \boldsymbol{E}^{-n}_{\rm EOS}(t)], \quad (1)$$

$$\boldsymbol{E}^{\rm AHE}_{\rm EOS}(t) = \frac{1}{2}[\boldsymbol{E}^{+n}_{\rm EOS}(t) - \boldsymbol{E}^{-n}_{\rm EOS}(t)]. \quad (2)$$

In Figs. 4(a) and 4(b) we decompose the two waveforms, $\boldsymbol{E}^{\rm UDM}_{\rm EOS}(t)$ and $\boldsymbol{E}^{\rm AHE}_{\rm EOS}(t)$ for Fe films with different thicknesses. The solid lines and dashed lines correspond to the measurements with $+H$ and $-H$, respectively. We notice that the polarity of the waveform for the UDM contribution is opposite to that for the AHE contribution. Figures 4(c) and 4(d) show the peak amplitudes of $\boldsymbol{E}^{\rm UDM}_{\rm EOS}(t)$ and $\boldsymbol{E}^{\rm AHE}_{\rm EOS}(t)$ plotted as functions of Fe thickness. For both $\pm H$ the THz emission via the UDM mechanism, $\boldsymbol{E}^{\rm UDM}_{\rm EOS}$ shows a linear dependence on the Fe thickness. The evolution of amplitude and frequency of $\boldsymbol{E}^{\rm UDM}_{\rm EOS}$ can be a probe for the varying demagnetization processes of the Fe film.[49] In terms of the THz emission via the AHE mechanism, $\boldsymbol{E}^{\rm AHE}_{\rm EOS}$ reaches a maximum for 5-nm-thick Fe and then decreases monotonically when the thickness further increases. The thickness dependence of THz emission is a combined effect of optical/THz absorption, backflow current generation and conversion.[39]

Finally, we notice that the THz waveforms for 4-nm and 5-nm-thick Fe films have the same polarity, which is different from the THz emission driven by a femtosecond Ti:sapphire oscillator. THz emission changes the polarity sign for 4-nm and 5-nm-thick Fe, consistent with the DC ANE voltages. This provides experimental evidence of the ANE mechanism THz emission due to the ultrafast temperature gradient created by the oscillator femtosecond laser.[50] It is noted that the AHE voltages have the same sign for the 4-nm and 5-nm-thick samples, which is in line with the unchanged sign of the THz emission signals. Based on the calculation results in our previous work,[50] the electron temperature gradient ∇T via ANE is proportional to the pump fluence below $0.2\,{\rm mJ\cdot cm^{-2}}$, but deviates from the linear dependence and becomes smaller at high pump fluences (see Fig. S7 in Ref. [50]). Thus, the relative contribution to the THz emission from ANE is small at high pump fluences. Our experimental results and calculations are also consistent with the observation of unchanged THz polarity of Fe (10 nm) upon sample flipping, in which a pump fluence of $1.1\,{\rm mJ\cdot cm^{-2}}$ was used.[34] Our measurement demonstrates that both UDM and AHE mechanisms dominate THz emission from Fe films driven by a Ti:sapphire regenerative amplifier.

To summarize, by using THz emission spectroscopy and an associated symmetry analysis we have demonstrated UDM- and AHE-driven THz emission in single-layer Fe films. Based on the magnetic field, pumping geometry and thickness dependences of THz emission from single-layer Fe films, we separate the AHE and UDM mechanisms. We compare the polarities of THz emission from 4-nm and 5-nm-thick samples: they have the same polarity, which indicates that the contribution from the ANE is unobservable for pumping by a Ti:sapphire regenerative amplifier. Our results not only enrich understanding of THz electromagnetic emission but also provide a practical way to access laser-induced ultrafast spin dynamics in magnetic structures.

Acknowledgements. This work was supported by the National Key Research and Development Program of China (Grant Nos. 2023YFF0719200 and 2022YFA1404004), the National Natural Science Foundation of China (Grant Nos. 61988102, 62322115, 61975110, and 62335012), the 111 Project (Grant No. D18014), the Key Project supported by Science and Technology Commission Shanghai Municipality (Grant No. YDZX20193100004960), Science and Technology Commission of Shanghai Municipality (Grant No. 22JC1400200), and General Administration of Customs People's Republic of China (Grant No. 2019HK006).

References

[1] Beaurepaire E, Merle J C, Daunois A, and Bigot J Y 1996 *Phys. Rev. Lett.* **76** 4250
[2] Beaurepaire E, Turner G M, Harrel S M, Beard M C, Bigot J Y, and Schmuttenmaer C A 2004 *Appl. Phys. Lett.* **84** 3465
[3] Kimel A V, Kirilyuk A, Usachev P A, Pisarev R V, Balbashov A M, and Rasing T 2005 *Nature* **435** 655
[4] Kirilyuk A, Kimel A V, and Rasing T 2010 *Rev. Mod. Phys.* **82** 2731; [Erratum: 2016 *Rev. Mod. Phys.* **88** 039904]
[5] Afanasiev D, Hortensius J R, Ivanov B A, Sasani A, Bousquet E, Blanter Y M, Mikhaylovskiy R V, Kimel A V, and Caviglia A D 2021 *Nat. Mater.* **20** 607
[6] Wu N, Zhang S J, Wang Y X, and Meng S 2023 *Prog. Surf. Sci.* **98** 100709
[7] Elliott P, Müller T, Dewhurst J K, Sharma S, and Gross E K U 2017 *Sci. Rep.* **6** 38911
[8] Chumak A V, Vasyuchka V I, Serga A A, and Hillebrands B 2015 *Nat. Phys.* **11** 453
[9] Fan X F, Hehn M, Wei G D, Malinowski G, Huang T X, Xu Y, Zhang B Y, Zhang W, Lin X Y, Zhao W S, and Mangin S 2022 *Adv. Electron. Mater.* **8** 2200114
[10] Seifert T S, Cheng L, Wei Z X, Kampfrath T, and Qi J B 2022 *Appl. Phys. Lett.* **120** 180401
[11] Windsor Y W, Lee S E, Zahn D, Borisov V, Thonig D, Kliemt K, Ernst A, Schussler-Langeheine C, Pontius N, Staub U, Krellner C, Vyalikh D V, Eriksson O, and Rettig L 2022 *Nat. Mater.* **21** 514
[12] Ji B Y, Jin Z M, Wu G J, Li J G, Wan C H, Han X F, Zhang Z Z, Ma G H, Peng Y, and Zhu Y M 2023 *Appl. Phys. Lett.* **122** 111104
[13] He J J, Li S, Frauenheim T, and Zhou Z B 2023 *Nano Lett* **23** 8348
[14] Kang K, Omura H, Yesudas D, Lee O, Lee K J, Lee H W, Taniyama T, and Choi G M 2023 *Nat. Commun.* **14** 3619
[15] Ferguson B and Zhang X C 2002 *Nat. Mater.* **1** 26
[16] Koch M, Mittleman D M, Ornik J, and Castro-Camus E 2023 *Nat. Rev. Methods Primers* **3** 48
[17] Peng Q F, Peng Z Y, Lang Y, Zhu Y L, Zhang D W, Lü Z H, and Zhao Z X 2022 *Chin. Phys. Lett.* **39** 053301

[18] Wu X J 2023 *Chin. Phys. Lett.* **40** 054001
[19] Peng Y, Shi C J, Zhu Y M, Gu M, and Zhuang S L 2020 *PhotoniX* **1** 12
[20] Peng Y, Huang J L, Luo J, Yang Z F, Wang L P, Wu X, Zang X F, Yu C, Gu M, Hu Q, Zhang X C, Zhu Y M, and Zhuang S L 2021 *PhotoniX* **2** 12
[21] Jia G R, Zhao D X, Zhang S S, Yue X W, Qin C C, Jiao Z Y, and Bian X B 2023 *Chin. Phys. Lett.* **40** 103202
[22] Xu X, Huang Y D, Zhang Z L, Liu J L, Lou J, Gao M X, Wu S Y, Fang G Y, Zhao Z X, Chen Y P, Sheng Z M, and Chang C 2023 *Chin. Phys. Lett.* **40** 045201
[23] Liu Y P, Shi J C, and Chen C Y 2022 *Chin. Phys. Lett.* **39** 018701
[24] Zhu Y, Zang X F, Chi H X, Zhou Y W, Zhu Y M, and Zhuang S L 2023 *Light: Adv. Manufact.* **4** 104
[25] Baierl S, Mentink J H, Hohenleutner M, Braun L, Do T M, Lange C, Sell A, Fiebig M, Woltersdorf G, Kampfrath T, and Huber R 2016 *Phys. Rev. Lett.* **117** 197201
[26] Lu J, Li X, Hwang H Y, Ofori-Okai B K, Kurihara T, Suemoto T, and Nelson K A 2017 *Phys. Rev. Lett.* **118** 207204
[27] Qiu H S, Seifert T S, Huang L, Zhou Y J, Kaspar Z, Zhang C H, Wu J B, Fan K B, Zhang Q, Wu D, Kampfrath T, Song C, Jin B B, Chen J, and Wu P H 2023 *Adv. Sci.* **10** 2300512
[28] Li Z S, Jiang Y X, Jin Z M, Li Z Y, Lu X Y, Ye Z J, Pang J Y, Xu Y B, and Peng Y 2022 *Nanomaterials* **12** 4267
[29] Cheng L, Wang X B, Yang W F, Chai J W, Yang M, Chen M J, Wu Y, Chen X X, Chi D Z, Goh K E J, Zhu J X, Sun H D, Wang S J, Song J C W, Battiato M, Yang H, and Chia E E M 2019 *Nat. Phys.* **15** 347
[30] Comstock A, Biliroglu M, Seyitliyev D, McConnell A, Vetter E, Reddy P, Kirste R, Szymanski D, Sitar Z, Collazo R, Gundogdu K, and Sun D L 2023 *Adv. Opt. Mater.* **11** 2201535
[31] Huang L, Lee S H, Kim S D, Shim J H, Shin H J, Kim S, Park J, Park S Y, Choi Y S, Kim H J, Hong J I, Kim D E, and Kim D H 2020 *Sci. Rep.* **10** 15843
[32] Seifert T S, Go D, Hayashi H, Rouzegar R, Freimuth F, Ando K, Mokrousov Y, and Kampfrath T 2023 *Nat. Nanotechnol.* **18** 1132
[33] Pettine J, Padmanabhan P, Sirica N, Prasankumar R P, Taylor A J, and Chen H T 2023 *Light Sci. Appl.* **12** 133
[34] Zhang W T, Maldonado P, Jin Z M, Seifert T S, Arabski J, Schmerber G, Beaurepaire E, Bonn M, Kampfrath T, Oppeneer P M, and Turchinovich D 2020 *Nat. Commun.* **11** 4247
[35] Kampfrath T, Battiato M, Maldonado P, Eilers G, Nötzold J, Mährlein S, Zbarsky V, Freimuth F, Mokrousov Y, Blügel S, Wolf M, Radu I, Oppeneer P M, and Münzenberg M 2013 *Nat. Nanotechnol.* **8** 256
[36] Jin Z M, Guo Y Y, Peng Y, Zhang Z Y, Pang J Y, Zhang Z Z, Liu F, Ye B, Jiang Y X, Ma G H, Zhang C, Balakin A V, Shkurinov A P, Zhu Y M, and Zhuang S L 2023 *Adv. Phys. Res.* **2** 2370003
[37] Zhou C, Liu Y P, Wang Z, Ma S J, Jia M W, Wu R Q, Zhou L, Zhang W, Liu M K, Wu Y Z, and Qi J 2018 *Phys. Rev. Lett.* **121** 086801
[38] Jungfleisch M B, Zhang Q, Zhang W, Pearson J E, Schaller R D, Wen H D, and Hoffmann A 2018 *Phys. Rev. Lett.* **120** 207207
[39] Zhang Q, Luo Z Y, Li H, Yang Y M, Zhang X H, and Wu Y H 2019 *Phys. Rev. Appl.* **12** 054027
[40] Liu Y S, Cheng H Y, Xu Y, Vallobra P, Eimer S, Zhang X Q, Wu X J, Nie T X, and Zhao W S 2021 *Phys. Rev. B* **104** 064419
[41] Mottamchetty V, Rani P, Brucas R, Rydberg A, Svedlindh P, and Gupta R 2023 *Sci. Rep.* **13** 5988
[42] Su G, Li Y F, Hou D Z, Jin X F, Liu H F, and Wang S G 2014 *Phys. Rev. B* **90** 214410
[43] Yang Y M, Luo Z Y, Wu H J, Xu Y J, Li R W, Pennycook S J, Zhang S F, and Wu Y H 2018 *Nat. Commun.* **9** 2255
[44] Huang L, Kim J W, Lee S H, Kim S D, Tien V, Shinde K P, Shim J H, Shin Y, Shin H J, Kim S, Park J, Park S Y, Choi Y S, Kim H J, Hong J I, Kim D E, and Kim D H 2019 *Appl. Phys. Lett.* **115** 142404
[45] Jiang Y X, Li Z S, Li Z Y, Jin Z M, Lu X Y, Xu Y B, Peng Y, and Zhu Y M 2023 *Opt. Lett.* **48** 2054
[46] Jin Z M, Peng Y, Ni Y Y, Wu G J, Ji B Y, Wu X, Zhang Z Z, Ma G H, Zhang C, Chen L, Balakin A V, Shkurinov A P, Zhu Y M, and Zhuang S L 2022 *Laser Photon. Rev.* **16** 2100688
[47] Rouzegar R, Brandt L, Nádvorník L, Reiss D A, Chekhov A L, Gueckstock O, In C, Wolf M, Seifert T S, Brouwer P W, Woltersdorf G, and Kampfrath T 2022 *Phys. Rev. B* **106** 144427
[48] Jiménez-Cavero P, Gueckstock O, Nádvorník L, Lucas I, Seifert T S, Wolf M, Rouzegar R, Brouwer P W, Becker S, Jakob G, Kläui M, Guo C Y, Wan C H, Han X F, Jin Z M, Zhao H, Wu D, Morellón L, and Kampfrath T 2022 *Phys. Rev. B* **105** 184408
[49] Wang C, Chen Y P, Xia T H, Wang L Z, Qi R Z, Zhang J Y, and Sheng Z M 2023 *Appl. Phys. Lett.* **123** 152403
[50] Feng Z, Tan W, Jin Z M, Chen Y J, Zhong Z F, Zhang L, Sun S, Tang J, Jiang Y X, Wu P H, Cheng J, Miao B F, Ding H F, Wang D C, Zhu Y M, Guo L, Shin S, Ma G H, Hou D Z, and Huang S Y 2023 *Nano Lett.* **23** 8171